

## A large-area and contamination-free graphene transistor for liquid-gated sensing applications

Yung Yu Wang<sup>1</sup> and Peter J. Burke<sup>2</sup>

<sup>1</sup>Department of Chemical Engineering and Materials Science, University of California, Irvine, California 92697, USA

<sup>2</sup>Department of Electrical Engineering and Computer Science, University of California, Irvine, California 92697, USA

(Received 17 December 2012; accepted 11 July 2013; published online 29 July 2013)

We present a simple, low-cost, large area, and contamination-free monolayer graphene field-effect transistor for liquid-gated sensing applications. The graphene surface does not require any photoresist including the commonly used polymethylmethacrylate, thus avoiding possible contamination and mobility degradation. We also examine the effects of different etching solutions and concentrations on the Dirac point of graphene. With optimal device fabrication recipe, we demonstrate the device's capability to sense different KCl concentrations and pH values under liquid gating configuration. Additionally, using polydimethylsiloxane as substrates holds an advantage of enabling simple integration between microfluidic systems and graphene for chemical and biological sensor applications. © 2013 AIP Publishing LLC. [<http://dx.doi.org/10.1063/1.4816764>]

Graphene, an atom-thick layer of  $sp^2$ -bonded hexagonal carbon<sup>1,2</sup> due to its uniquely two-dimensional surface, is an advanced candidate for chemical and biological sensors.<sup>3,4</sup> Recently, several graphene synthesis methods have been developed, such as chemical vapor deposition (CVD) on metal substrate Ni (Ref. 5) and Cu.<sup>6</sup> Chemical vapor deposition has been demonstrated as a reliable method for self-limited growth of single-layer graphene on copper foil.<sup>6</sup> However, the sensor fabrication and graphene transfer usually involve the use of photoresists and polymethylmethacrylate (PMMA) on graphene surface, causing contamination<sup>7</sup> and n-type doping.<sup>8</sup> Although recent works have shown that using thermal treatment about 300–400 °C in  $H_2/Ar$  atmosphere<sup>7</sup> or in high-vacuum<sup>9,10</sup> can remove most of photoresists and PMMA, the remaining residues could still hamper sensor applications. Annealing at high temperature may lead to heavy hole doping and mobility degradation of graphene.<sup>11</sup> Moreover, high temperature, post transfer anneals are not compatible with polymer substrates such as polydimethylsiloxane (PDMS), widely used in microfluidics and sensing applications.

Although the transfer of graphene using PDMS has already been reported in existing literatures,<sup>12–19</sup> the PDMS is used as stamp to print graphene on the different substrates like  $SiO_2$  wafer. There is no graphene field-effect transistors (FETs) made directly on PDMS substrates for sensing applications. While transfer printing of graphene can provide a contamination-free method for device fabrication, it may only work on multilayer and small area graphene with 100  $\mu m$  for the channel length of graphene transistors. Because the transfer printing method is totally dependent on the surface adhesion between the graphene film and the target substrate, it is difficult to transfer large area monolayer graphene. Hence, these problems may impede the applications of graphene-based sensors.

In this work, we present a simple and low-cost fabrication of graphene field-effect transistor on PDMS which

provides contamination-free and large area monolayer graphene film for liquid-gated sensing applications. Single layer graphene is transferred by PDMS; then, the PDMS is directly used as substrate for device fabrication. The channel length of the transistors can be larger than 5 mm. This device avoids any chemical contamination during graphene transfer and fabrication. Therefore, a clean and high quality graphene surface is provided for investigation in variety of chemical and biological materials.

Figure 1 shows a schematic illustration of transfer process. We physically attached a PDMS block on a commercial CVD-grown single layer graphene on copper foil (ACS Material). Then PDMS/graphene/foil block was floated on the surface of 0.05 g/ml ammonium persulfate solution (Aldrich,  $\geq 98\%$ ) to etch copper foil. After the copper was etched, the PDMS/graphene block was rinsed with deionized water several times.

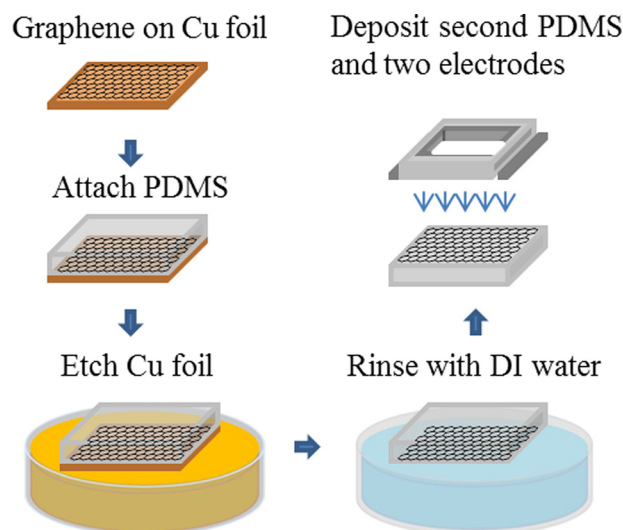


FIG. 1. Schematic illustration of graphene film in transfer, etch, and fabrication on PDMS substrate.

Then the second layer of PDMS with open well was employed to hold electrolyte solution. Finally, source and drain electrodes were directly deposited by silver conductive paint.<sup>20</sup>

Figure 2(a) is an optical image of monolayer graphene with size  $1\text{ cm} \times 1\text{ cm}$  on a PDMS substrate. Figure 2(b) shows Raman spectrum (532 nm laser wavelength) of graphene transfer-printed from PDMS onto  $\text{SiO}_2/\text{Si}$  wafer. Because PDMS substrate will show some noise peaks on the Raman spectrum,<sup>20</sup> we decide to transfer and print graphene onto the  $\text{SiO}_2/\text{Si}$  wafer for Raman investigation. The G and 2D peaks of graphene film are positioned at  $\sim 1566\text{ cm}^{-1}$  and  $\sim 2675\text{ cm}^{-1}$ , respectively. The ratio of the integrated intensity of G band to 2D band is 0.3, which suggests the graphene film to be monolayer.<sup>21</sup> Also, a negligible defect-related D band is at  $1330\text{ cm}^{-1}$ , which indicates the defects caused during transfer printing from PDMS to  $\text{SiO}_2/\text{Si}$  wafer. We also used atomic force microscopy to examine the thickness of the graphene film. The thickness of our graphene film is about 0.5 nm in our previous work.<sup>22</sup> From these results, the film on the PDMS substrate shows a high quality monolayer graphene.<sup>23</sup> Figure 2(c) presents a typical AFM image of single layer graphene surface on PDMS substrate. There are some wrinkles in the AFM image. Those wrinkles are formed during the cooling step in the CVD-growth process due to the difference of thermal coefficients between the graphene film and copper foil. Except those wrinkles, no residues are observed, which indicates the graphene surface is very clean. Figure 2(d) shows a scanning electron microscopy (SEM) image of single layer graphene on the PDMS substrate. Then sample is observed directly under scanning electron microscopy without any coating. Graphene sheet is complete over the PDMS substrate.

Figure 3(a) presents the device layout of liquid gated graphene transistor. The source and drain electrodes were deposited by silver paint, and PDMS with a hole was used to insulate the ionic solution from the electrodes. The graphene

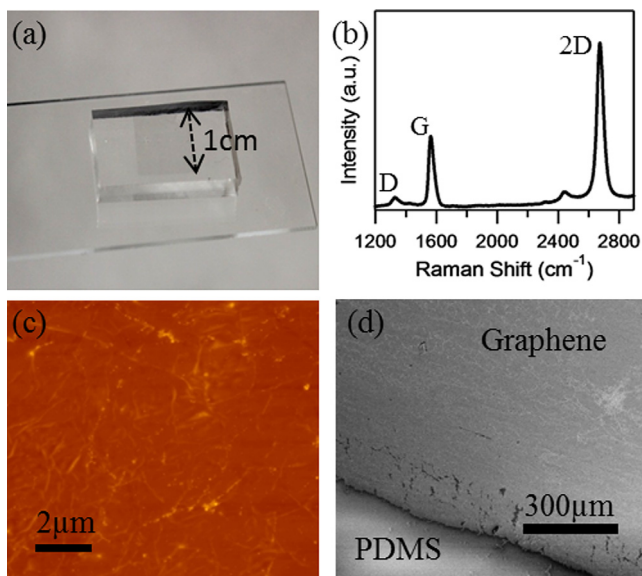


FIG. 2. (a) Optical image of monolayer graphene on PDMS substrate. (b) Raman spectrum of monolayer graphene transfer-printed from PDMS to  $\text{SiO}_2/\text{Si}$  substrate. (c) AFM image of monolayer graphene surface on PDMS substrate. (d) SEM image of monolayer graphene border on PDMS substrate.

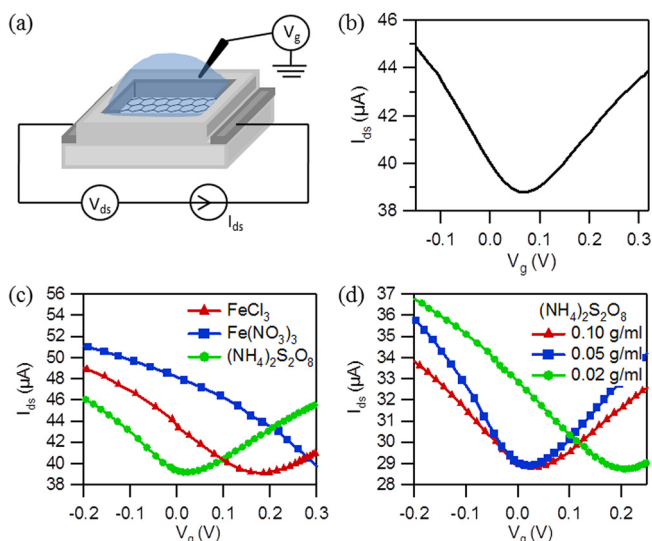


FIG. 3. (a) Schematic illustration of single layer graphene field-effect transistor on PDMS substrate. (b) The drain-source current vs liquid gate voltage characteristics of single layer graphene FETs on PDMS substrate in 0.1 M phosphate buffer at pH 7 with 100 mM KCl and  $V_{ds} = 0.1\text{ V}$ . (c) The effect of graphene FETs' transfer curves in different etching solution  $\text{FeCl}_3$ ,  $\text{Fe}(\text{NO}_3)_3$ , and  $(\text{NH}_4)_2\text{S}_2\text{O}_8$ . (d) The effect of graphene FETs' transfer curves in different concentration of  $(\text{NH}_4)_2\text{S}_2\text{O}_8$  (0.1 g/ml, 0.05 g/ml, and 0.02 g/ml).

film was gated through a  $\text{Ag}/\text{AgCl}$  reference electrode in the ion solution. Figure 3(b) shows the liquid-gated ambipolar field-effect characteristics of the graphene transistor ( $I_{ds}$  vs  $V_g$ ,  $V_{ds} = 100\text{ mV}$ ) in 100 mM KCl solution. The transfer characteristics present a V-shaped p- to n-type transition. The mobility of the device can be calculated from the equation  $\mu = (L/WC_g V_d)(\Delta I_d/\Delta V_g)$ ,<sup>8</sup> where  $L$  and  $W$  are the channel length = 0.3 cm and width = 0.6 cm, and  $C_g$  capacitance of graphene is  $57\text{ nF cm}^{-2}$ . The liquid-gated hole and electron mobility are  $2053\text{ cm}^2/(\text{V s})$  and  $1429\text{ cm}^2/(\text{V s})$ , respectively. The leakage current is less than 15 nA in the range of applied gate voltage.<sup>20</sup> The contact resistance between silver paste and graphene is about  $917\ \Omega$ .<sup>20</sup> Although the contact resistance can affect the device total electrical characteristics if it is comparable to the channel resistance such as in short channel devices,<sup>24</sup> in our case the contact resistance is much less than the channel resistance (we have a very long channel) and so does not affect the extrapolated mobility calculation. More quantitatively, it is well known in the device physics field that if the transconductance–contact resistance product is less than one (which is the case for our measurements), it does not affect the total (measured) transconductance.

In order to understand the effect of different etching solution on graphene's Dirac point during the transfer process, the copper foil is etched by three different solutions,  $\text{FeCl}_3$  (0.05 g/ml),  $\text{Fe}(\text{NO}_3)_3$  (0.05 g/ml), and  $(\text{NH}_4)_2\text{S}_2\text{O}_8$  (0.05 g/ml) for 5 h. Because of the ambipolar characteristics of graphene, we can see the field-effect response V-shaped which is both hole and electron conductance in the graphene FETs. For a perfect and contamination-free graphene device, the Dirac point should close to zero. When the graphene surface has adsorbed any chemicals, the Dirac point of graphene will shift to positive or negative gate voltage. By observing the shift of the Dirac point, we can determine the change of

graphene surface. Figure 3(c) is drain-source current variation of graphene FETs etched by  $\text{FeCl}_3$  (red),  $\text{Fe}(\text{NO}_3)_3$  (blue), and  $(\text{NH}_4)_2\text{S}_2\text{O}_8$  (green) as a function of the gate voltage in 0.1 mM phosphate buffer at pH 7 with 100 mM KCl and 100 mV drain source voltage. A linear blue curve is observed across the liquid gate voltage range. This indicates that the graphene sheet adsorbs the  $\text{NO}_3^-$  ions during the etching process. This n-type doping will make the Fermi level of graphene shift to valence band. In order to see the Dirac point, the more positive gate voltage should be applied. It is difficult to get rid of this contamination by rinsing with deionized water even for a longer time. Graphene films which are etched by  $\text{FeCl}_3$  and  $(\text{NH}_4)_2\text{S}_2\text{O}_8$  show V-shaped  $I_{\text{ds}}-V_{\text{g}}$  curves (red and green curves, respectively). However, the Dirac point of the red curve is around 0.18 V. This shows that the graphene film has minor n-type doping contamination by  $\text{FeCl}_3$  etching solution. The reason is the adsorption of  $\text{Cl}^-$  ions on the graphene sheet during the etching process. This negative ions doping will shift the Fermi level of graphene to valence band. Then the Dirac point will shift to more positive gate voltage. We do not see any improvement upon rinse with deionized water for a longer time. Finally, the green curve has Dirac point around 0.02 V. This indicates graphene film etched by  $(\text{NH}_4)_2\text{S}_2\text{O}_8$  has less doping contamination.

In Figure 3(d), we show drain-source current variation of graphene FETs etched by different concentrations of solution  $(\text{NH}_4)_2\text{S}_2\text{O}_8$  (0.1 g/ml red, 0.05 g/ml blue, and 0.02 g/ml green) as function of the gate voltage in 0.1 mM phosphate buffer at pH 7 with 100 mM KCl and 100 mV drain source voltage. Three different concentrations all show V-shapes in the range of applied gate voltage. Only the green curve's Dirac point has right shift around 0.2 V. This shows 0.02 g/ml  $(\text{NH}_4)_2\text{S}_2\text{O}_8$  concentration will cause minor n-type doping contamination on graphene surface, due to the fact that the lower concentration needs a longer etching time to get rid of the copper foil. Longer etching time may lead to some negative ions adsorption on graphene film. Therefore, the Dirac point of graphene has positive shift. In the higher concentration 0.1 g/ml and 0.05 g/ml, both of them have Dirac point around 0.04 V and 0.02 V, respectively. Because of high concentration, they can quickly etch away copper foil without causing n-type doping in the graphene film. However, while comparing to the hole and electron mobility, blue curve (0.05 g/ml) has hole and electron mobility  $1922 \text{ cm}^2/(\text{V s})$  and  $1375 \text{ cm}^2/(\text{V s})$ , which are higher than red curve's (0.1 g/ml) hole and electron mobility  $1351 \text{ cm}^2/(\text{V s})$  and  $1024 \text{ cm}^2/(\text{V s})$ , respectively. Since higher  $(\text{NH}_4)_2\text{S}_2\text{O}_8$  concentration (0.1 g/ml) has more rapid reaction during etching process, this will cause some degradation of the graphene quality. We conclude the etching solution  $(\text{NH}_4)_2\text{S}_2\text{O}_8$  (0.05 g/ml) is the optimize concentration for our device fabrication without any doping contamination and mobility degradation.

In order to demonstrate the sensing applications of our devices, we investigated our devices with liquid gating in different KCl concentrations and pH values. Figure 4(a) shows drain-source current as function of gate voltage in different KCl concentrations. The  $I_{\text{ds}}-V_{\text{g}}$  curve is shifted to left while the ionic strength is increased. This indicates an electrostatic gating effect happens. The electrostatic gating effect

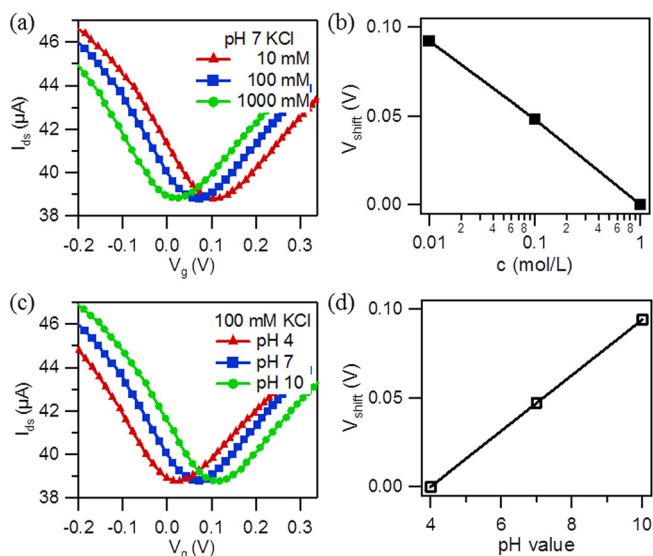


FIG. 4. (a) The drain-source current vs liquid gate voltage characteristics of graphene FET in 0.1 mM phosphate buffer at pH 7 with 10 mM KCl (red), 100 mM KCl (blue), and 1 M KCl (green). (b) Shift of the  $I_{\text{ds}}-V_{\text{g}}$  curves in (a),  $V_{\text{shift}}$  with respect to the 1 M KCl, as a function of the KCl concentration. (c) The drain-source current vs liquid gate voltage characteristic of graphene FET in 0.1 mM phosphate buffer with 100 mM KCl at pH 4 (red), pH 7 (blue), and pH 10 (green). (d) Shift of the  $I_{\text{ds}}-V_{\text{g}}$  curves in (c),  $V_{\text{shift}}$  with respect to the pH 4, as a function of the pH value.

is generated by surface potential at the graphene-liquid interface. When the negative surface charge which is screened by ions attracts mobile positive charges to the graphene-liquid interface, the negative surface potential is formed. These positive charges are both positive charges (holes) in the graphene and positive ions in the electrical double layer in solution. At higher ionic strength, the electrical double layer is compressed which will decrease the negative surface potential. Then the lesser positive gate voltage is required to compensate this negative surface potential. Therefore, the positive shift of the Dirac point becomes smaller. This result is in agreement with previous studies.<sup>25-27</sup> Figure 4(b) is  $V_{\text{shift}}$  of Figure 4(a) as a function of KCl concentration with respect to 1 M KCl. In the curve, the  $V_{\text{shift}}$  is linear to  $\log([\text{KCl}])$  over the 3 orders of magnitude concentration change.

Figure 4(c) shows drain-source current as function of gate voltage in different pH values. An increase in pH from pH 4 to pH 10 causes a shift toward more positive  $V_{\text{g}}$ . At higher pH, there is more adsorption of  $\text{OH}^-$  ions on graphene surface. Then the negative surface potential becomes larger. The higher positive gate voltage is applied to compensate this negative surface potential. Thus, the Dirac point of graphene will shift to more positive gate voltage. This result also observed in other reports.<sup>3,4</sup> Figure 4(d) is  $V_{\text{shift}}$  of Figure 4(c) as a function of pH value with respect to pH 4. This curve also shows the  $V_{\text{shift}}$  is linear to change of pH value. Our work is different than previous studies<sup>3,4,16-18</sup> from using direct transfer graphene FETs device without any contamination of photoresists and PMMA. By operating these two experiments, our graphene FET shows highly potential for chemical and biological sensing applications.

In conclusion, we have demonstrated a simple, low-cost, large area, and contamination-free monolayer graphene

field-effect transistor on PDMS substrates for liquid-gated sensing applications. This device not only avoids the contamination of photoresists and PMMA but also prevents the mobility degradation of annealing process on the graphene film. Therefore, our graphene field-effect transistors present a large area and contamination-free clean monolayer graphene surface. This clean graphene surface FET can provide a platform to study the effects of many different chemical and biological materials with monolayer graphene by liquid-gated ambipolar characteristics. In addition, we investigated the effects of graphene's Dirac point in different etching solutions and concentrations on graphene film. We also demonstrated the liquid-gated sensing applications for different KCl concentrations and pH values. We believe that our devices have substantial potential for chemical and biological liquid-gated sensor applications.

This work was funded by the Army Research Office through ARO-MURI program and ARO-Core grants (MURI W911NF-11-1-0024, ARO W911NF-09-1-0319, and DURIP W911NF-11-1-0315).

<sup>1</sup>A. K. Geim, *Science* **324**, 1530 (2009).

<sup>2</sup>K. S. Novoselov, V. I. Fal'ko, L. Colombo, P. R. Gellert, M. G. Schwab, and K. Kim, *Nature (London)* **490**, 192 (2012).

<sup>3</sup>P. K. Ang, W. Chen, A. T. S. Wee, and K. P. Loh, *J. Am. Chem. Soc.* **130**, 14392 (2008).

<sup>4</sup>Y. Ohno, K. Maehashi, Y. Yamashiro, and K. Matsumoto, *Nano Lett.* **9**, 3318 (2009).

<sup>5</sup>Q. Yu, J. Lian, S. Siriponglert, H. Li, Y. P. Chen, and S. S. Pei, *Appl. Phys. Lett.* **93**, 113103 (2008).

<sup>6</sup>X. Li, W. Cai, J. An, S. Kim, J. Nah, D. Yang, R. Piner, A. Velamakanni, I. Jung, E. Tutuc, S. K. Banerjee, L. Colombo, and R. S. Ruoff, *Science* **324**, 1312 (2009).

<sup>7</sup>Y. Dan, Y. Lu, N. J. Kybert, Z. Luo, and A. T. C. Johnson, *Nano Lett.* **9**, 1472 (2009).

<sup>8</sup>V. Geringer, D. Subramaniam, A. K. Michel, B. Szafranek, D. Schall, A. Georgi, T. Mashoff, D. Neumaier, M. Liebmann, and M. Morgenstern, *Appl. Phys. Lett.* **96**, 82114 (2010).

<sup>9</sup>A. Pirkle, J. Chan, A. Venugopal, D. Hinojos, C. W. Magnuson, S. McDonnell, L. Colombo, E. M. Vogel, R. S. Ruoff, and R. M. Wallace, *Appl. Phys. Lett.* **99**, 122108 (2011).

<sup>10</sup>S. Chen, W. Cai, D. Chen, Y. Ren, X. Li, Y. Zhu, J. Kang, and R. S. Ruoff, *New J. Phys.* **12**, 125011 (2010).

<sup>11</sup>Z. Cheng, Q. Zhou, C. Wang, Q. Li, C. Wang, and Y. Fang, *Nano Lett.* **11**, 767 (2011).

<sup>12</sup>X. Li, W. Cai, I. H. Jung, J. H. An, D. Yang, A. Velamakanni, R. Piner, L. Colombo, and R. S. Ruoff, *ECS Trans.* **19**, 41 (2009).

<sup>13</sup>M. J. Allen, V. C. Tung, L. Gomez, Z. Xu, L.-M. Chen, K. S. Nelson, C. Zhou, R. B. Kaner, and Y. Yang, *Adv. Mater.* **21**, 2098 (2009).

<sup>14</sup>K. S. Kim, Y. Zhao, H. Jang, S. Y. Lee, J. M. Kim, K. S. Kim, J.-H. Ahn, P. Kim, J.-Y. Choi, and B. H. Hong, *Nature (London)* **457**, 706 (2009).

<sup>15</sup>Y. Lee, S. Bae, H. Jang, S. Jang, S.-E. Zhu, S. H. Sim, Y. Il Song, B. H. Hong, and J.-H. Ahn, *Nano Lett.* **10**, 490 (2010).

<sup>16</sup>T. Oznucluer, E. Pince, E. O. Polat, O. Balci, O. Salihoglu, and C. Kocabas, *Appl. Phys. Lett.* **98**, 183101 (2011).

<sup>17</sup>S. J. Kang, B. Kim, K. S. Kim, Y. Zhao, Z. Chen, G. H. Lee, J. Hone, P. Kim, and C. Nuckolls, *Adv. Mater.* **23**, 3531 (2011).

<sup>18</sup>C. Y. Su, D. Fu, A. Y. Lu, K. K. Liu, Y. Xu, Z. Y. Juang, and L. J. Li, *Nanotechnology* **22**, 185309 (2011).

<sup>19</sup>J. Song, F.-Y. Kam, R.-Q. Png, W.-L. Seah, J.-M. Zhuo, G.-K. Lim, P. K. H. Ho, and L.-L. Chua, *Nat. Nanotechnol.* **8**, 356 (2013).

<sup>20</sup>See supplementary material at <http://dx.doi.org/10.1063/1.4816764> for optical image of monolayer graphene on PDMS substrate (Fig. S1), Raman spectra of PDMS and graphene/PDMS (Fig. S2), leakage current of graphene FET (Fig. S3), contact resistance of silver paste on graphene sheet (Fig. S4), and AFM topographic images of PMMA/graphene film (Fig. S5).

<sup>21</sup>D. Graf, F. Molitor, K. Ensslin, C. Stampfer, A. Jungen, C. Hierold, and L. Wirtz, *Nano Lett.* **7**, 238 (2007).

<sup>22</sup>N. Rouhi, S. Capdevila, D. Jain, K. Zand, Y. Wang, E. Brown, L. Jofre, and P. Burke, *Nano Res.* **5**, 667 (2012).

<sup>23</sup>C. J. Docherty, C. T. Lin, H. J. Joyce, R. J. Nicholas, L. M. Herz, L. J. Li, and M. B. Johnston, *Nat. Commun.* **3**, 1228 (2012).

<sup>24</sup>K. N. Parrish and D. Akinwande, *Appl. Phys. Lett.* **98**, 183505 (2011).

<sup>25</sup>I. Heller, S. Chatoor, J. Männik, M. A. G. Zevenbergen, C. Dekker, and S. G. Lemay, *J. Am. Chem. Soc.* **132**, 17149 (2010).

<sup>26</sup>F. Chen, Q. Qing, J. Xia, J. Li, and N. Tao, *J. Am. Chem. Soc.* **131**, 9908 (2009).

<sup>27</sup>A. B. Artyukhin, M. Stadermann, R. W. Friddle, P. Stroeve, O. Bakajin, and A. Noy, *Nano Lett.* **6**, 2080 (2006).

## SUPPLEMENTARY MATERIAL

### **A Large-Area and Contamination-Free Graphene Transistor for Liquid-Gated Sensing Applications**

Yung Yu Wang<sup>1</sup>, and Peter J. Burke<sup>2</sup>

Supporting Information 1: Monolayer graphene FET device

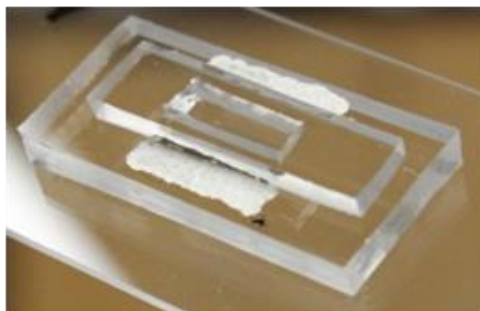


FIG. S1. Optical image of monolayer graphene FET on PDMS substrate.

This device is made by direct transfer process in figure 1. The top layer PDMS with the 1 cm  $\times$  0.3 cm hole is used to hold electrolyte solution. The liquid gate voltage is applied through a Ag/AgCl electrode to electrolyte solution. Beside the top layer PDMS are two source and drain electrodes which are deposited by silver conductive paint. The graphene film is transparent and under the top layer PDMS and the two electrodes. The size of graphene is 1 cm  $\times$  1 cm. The distance between two electrodes is 0.6 cm.

Supporting Information 2: Raman spectra

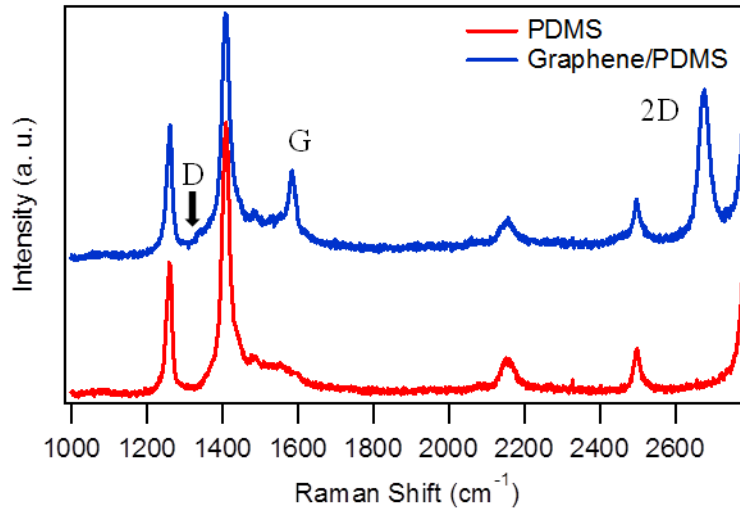


FIG. S2. Raman spectra of PDMS and graphene/PDMS.

After graphene is transferred onto PDMS, the sample is investigated by Raman spectroscopy. The blue curve is showing Raman spectrum of monolayer graphene on PDMS. The 2D and G peaks are observed as single layer graphene. The D peak is not present in the curve. This indicates transfer to the PDMS substrate does not generate any defects in the graphene film. The other noise peaks are not from the graphene film. They are generated by the PDMS substrate which is showed in the red curve. In order to avoid those noise peaks from PDMS, we transferred graphene film from PDMS to SiO<sub>2</sub>/Si substrate for Raman characterization. The Raman spectrum of the graphene film is showed in figure 2(b).

### Supporting Information 3: Leakage current of graphene FET

During the liquid gating measurement, we also examined the current from graphene device to solution. Figure S3(a) shows the schematic illustration of graphene device.  $I_g$  is gate current which is current flowing from graphene to Ag/AgCl reference electrode. Figure S3(b) presents this gate current vs gate voltage. The gate current is less than 15 nA at the maximum applied gate

voltage. This indicates that top layer PDMS can effectively insulate the electrolyte with two source and drain electrodes.

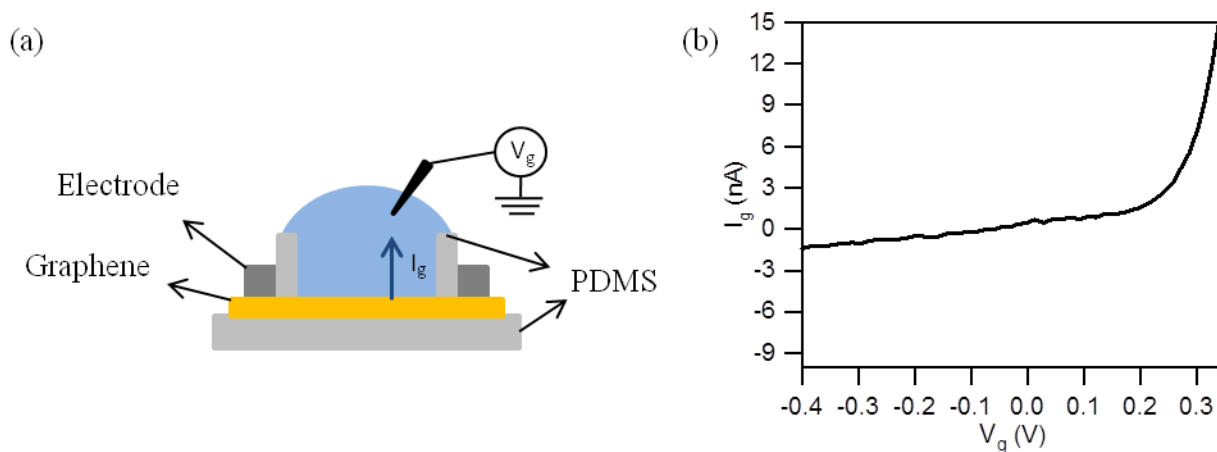


FIG. S3. (a) Schematic illustration of graphene device for investigation of gate current. (b) The liquid gate current vs liquid gate voltage characteristics of graphene FET in 0.1 mM phosphate buffer at pH 7 with 100 mM KCl.

#### Supporting Information 4: Contact resistance of silver paste on graphene sheet

For the contact resistance between silver paste and graphene sheet, the device is examined by two-electrode measurement. Figure 4S(a) is  $I_{ds}$  vs  $V_{ds}$  measurements of graphene on PDMS with different channel length from 1 mm to 5mm. From this figure, we can get the total contact resistance in response to different channel length. By drawing figure total resistance vs channel length in figure 4S(b), we can figure out the fitting line and the equation. From this equation, we can know that the contact resistance is about 917  $\Omega$ .

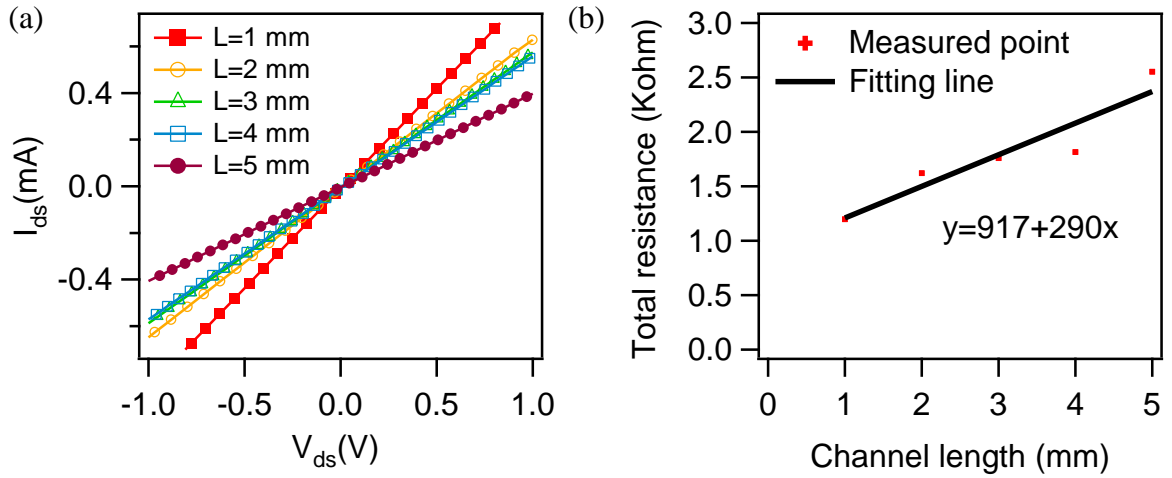


FIG. S4. (a)  $I_{ds}$  vs  $V_{ds}$  measurements of graphene on PDMS with different channel length. The two electrodes are painted by silver paste. (b) The device's total resistance vs channel length.

#### Supporting Information 5: AFM topographic images of PMMA/graphene film

In order to investigate graphene surface by PMMA transfer method, graphene/copper film was spin-coated by a 300 nm thickness of PMMA. After copper foil was etched, the PMMA/graphene film was transferred onto Si wafer and soaked in acetone for overnight. Figure 5S(a) is AFM topographic image of PMMA/graphene film after cleaned by acetone. The scan size is  $10 \mu\text{m} \times 10 \mu\text{m}$  and black bar is  $2 \mu\text{m}$ . The graphene surface is filled with PMMA residues. That means the acetone bath cannot effectively eliminate the PMMA. Figure 5S(b) is AFM line scan from figure 5S(a). The highest PMMA residue is 53 nm. Then this sample was annealed in forming gas (Ar 95% / H<sub>2</sub> 5%) at 400 °C for 3 hours. Figure 5S(c) is AFM topographic image of PMMA/graphene film annealed in forming gas. Most of PMMA residues are eliminated. But some 1 ~ 2  $\mu\text{m}$  width and 50 nm height PMMA residues are left which are showed in figure 5S(d). Our work avoids all of these contamination issues as discussed in the main text.

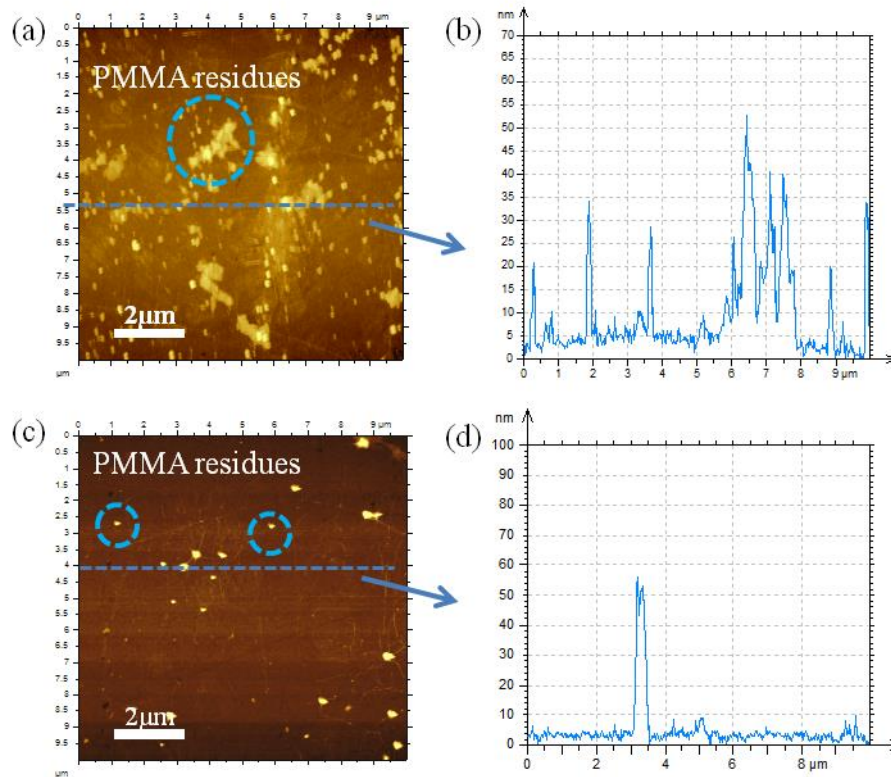


FIG. 5S. (a) AFM topographic image of PMMA/graphene film soaked in acetone bath for overnight. (b) AFM line scan from figure 5S(a). (c) AFM topographic image of PMMA/graphene film annealed in forming gas (Ar 95% / H<sub>2</sub> 5%) at 400 °C. (d) AFM line scan from figure 5S(c).

#### Supporting Information 6: AFM image of single layer graphene

Atomic force microscopy is employed to determine the number of the layer of CVD-grown graphene. The sample is prepared by spin-coating a layer of PMMA on graphene/copper film. After copper foil is etched, the PMMA/graphene film is transferred onto Si wafer. The PMMA is eliminated by acetone overnight and annealing in forming gas (Ar 95%/ H<sub>2</sub> 5%) at 400 °C for 3 hours. The thickness of this transferred graphene is about 0.5 nm. This indicates the CVD-grown graphene film is single layer. More detail and image are showed in our previous work<sup>22</sup>.